Multiscale Interactions in the Life Cycle of a Tropical Cyclone Simulated in a Global Cloud-System-Resolving Model. Part I: Large-Scale and Storm-Scale Evolutions*

HIRONORI FUDEYASU+ AND YUQING WANG

International Pacific Research Center, School of Ocean and Earth Science and Technology, University of Hawaii at Manoa, Honolulu, Hawaii

MASAKI SATOH

Atmosphere and Ocean Research Institute, University of Tokyo, Kashiwa, and Japan Agency for Marine Earth Science and Technology, Yokohama, Japan

TOMOE NASUNO

Japan Agency for Marine Earth Science and Technology, Yokohama, Japan

HIROAKI MIURA AND WATARU YANASE

Atmosphere and Ocean Research Institute, University of Tokyo, Kashiwa, Japan

(Manuscript received 22 April 2010, in final form 24 July 2010)

ABSTRACT

The Nonhydrostatic Icosahedral Atmospheric Model (NICAM), a global cloud-system-resolving model, successfully simulated the life cycle of Tropical Storm Isobel that formed over the Timor Sea in the austral summer of 2006. The multiscale interactions in the life cycle of the simulated storm were analyzed in this study. The large-scale aspects that affected Isobel's life cycle are documented in this paper and the corresponding mesoscale processes are documented in a companion paper.

The life cycle of Isobel was largely controlled by a Madden–Julian oscillation (MJO) event and the associated westerly wind burst (WWB). The MJO was found to have both positive and negative effects on the tropical cyclone intensity depending on the location of the storm relative to the WWB center associated with the MJO. The large-scale low-level convergence and high convective available potential energy (CAPE) downwind of the WWB center provided a favorable region to the cyclogenesis and intensification, whereas the strong large-scale stretching deformation field upwind of the WWB center may weaken the storm by exciting wavenumber-2 asymmetries in the eyewall and leading to the eyewall breakdown.

Five stages are identified for the life cycle of the simulated Isobel: the initial eddy, intensifying, temporary weakening, reintensifying, and decaying stages. The initial eddy stage was featured by small-scale/mesoscale convective cyclonic vortices developed in the zonally elongated rainband organized in the preconditioned environment characterized by the WWB over the Java Sea associated with the onset of an MJO event over the East Indian Ocean. As the MJO propagated eastward and the cyclonic eddies moved southward into an environment with weak vertical shear and strong low-level cyclonic vorticity, a typical tropical cyclone structure developed over the Java Sea, namely the genesis of Isobel. Isobel experienced an eyewall breakdown and a temporary weakening when it was located upwind of the WWB center as the MJO propagated southeastward and reintensified as its eyewall reformed as a result of the axisymmetrization of an inward spiraling outer rainband that originally formed downwind of the WWB center. Finally Isobel decayed as it approached the northwest coast of Australia.

* School of Ocean and Earth Science Technology Publication Number 7984 and International Pacific Research Center Publication Number 713.

+ Current affiliation: Faculty of Education and Human Sciences, Yokohama National University, Yokohama, Japan.

Corresponding author address: Dr. H. Fudeyasu, Yokohama National University, 79-1 Tokiwadai, Hodogaya-ku, Yokohama, Kanagawa 240-8501, Japan.
E-mail: fude@ynu.ac.jp

DOI: 10.1175/2010MWR3474.1

1. Introduction

To simulate and understand the life cycle of a tropical cyclone (TC), including genesis, intensification, structure and intensity changes, and decay, has long been a captivating subject at the frontier of science and remains challenging because of the complex multiscale interactions involved. The life cycle of a TC consists of a succession of stages starting from the establishment of a favorable environment to TC genesis. During the genesis stage, sustained convective activities, which may stem from a variety of processes in a favorable environment, develop into a surface mesoscale or synoptic vortex. Although the mesoscale processes in the genesis stage have been the least understood aspect of the life cycle of a TC, the climatological large-scale conditions favorable for TC genesis have been well known since Gray (1968, 1979). These include a sea surface temperature (SST) above about 26.5°C with a deep ocean mixed layer, a cyclonic low-level vorticity anomaly, weak and preferably easterly vertical shear, and a region of organized deep convection with a moistened mid-to-lower troposphere.

Previous studies have paid special attention to the role of the Madden–Julian oscillation (MJO; Madden and Julian 1971, 1972, 1994; Zhang 2005) in the organization of deep convection as a precursor to TC genesis (Liebmann et al. 1994; Maloney and Hartmann 2000a,b; Hall et al. 2001; Bessafi and Wheeler 2006; Barrett and Lance 2009). In addition to the MJO, various tropical/equatorial waves, such as the easterly waves, equatorial Rossby waves, mixed Rossby–gravity waves, can also modulate the large-scale vertical vorticity and vertical shear, thus significantly affecting TC genesis and life cycle over different ocean basins (Landsea 1993; Briegel and Frank 1997; Ritchie and Holland 1999; Thorncroft and Hodges 2001; Molinari and Vollaro 2000; Maloney and Hartmann 2001; Hall et al. 2001; Dickinson and Molinari 2002; Bessafi and Wheeler 2006; Frank and Roundy 2006).

The genesis stage is generally followed by an intensification stage. During this stage, the typical structure of a TC, such as the eye, eyewall, and spiral rainbands, would emerge. After its formation, the structure and intensity of a TC may be subject to changes due to both internal processes and external forcing (Wang and Wu 2004). Previous studies have shown that strong vertical shear may interrupt the intensification or weaken a TC by ventilating the warm core or triggering asymmetries in eyewall convection (Simpson and Riehl 1958; Gray 1968; McBride and Zehr 1981; Merrill 1988; Wang and Holland 1996; Bender 1997; Frank and Ritchie 1999, 2001; Wang et al. 2004; Black et al. 2002; Heymsfield et al. 2006; Zeng et al. 2007, 2008). Several internal dynamical processes can lead to an interruption of TC intensification or a weakening, such as the eyewall breakdown due to the interaction between spiral rainbands and eyewall convection (Wang 2002a,b) and the concentric eyewall cycle (Willoughby et al. 1982). The last stage of the life cycle of a TC is its decay under the effects of an unfavorable environment or when it moves over cold water or makes landfall, or its transition to become an extratropical cyclone.

Significant progress has been made in modeling TCs with high-resolution atmospheric models since Liu et al. (1997). The modeling studies have greatly improved our understanding of different stages of the life cycle of a TC. However, few studies have succeeded in simulating the whole life cycle of a TC because most high-resolution models are run in a limited area for several days and thus generally could not capture the life cycle of a TC that is always embedded in a large-scale flow with time scales longer than a week. Although two-way nesting with a moving mesh following a TC can reduce this discrepancy, the best way to avoid the problem completely is to run a global cloud-resolving model. The ever-increasing capability of powerful computers in recent years makes it possible to simulate the whole life cycle of a TC by running a global nonhydrostatic model at resolutions high enough to resolve cloud systems.

The first global cloud-system-resolving model, that is, the Nonhydrostatic Icosahedral Atmospheric Model (NICAM), with horizontal grid spacing of a few kilometers, simultaneously models cloud clusters, organized mesoscale convective systems, and the associated large-scale circulation, such as the MJO (Nasuno et al. 2007; Satoh et al. 2008). Miura et al. (2007) reported a successful simulation of a real MJO event in the austral summer 2006 in NICAM with realistic settings (hereinafter the MJO experiment). The MJO experiment reproduced the large-scale organized cloud systems, including the multiscale cloud clusters, in the convective phase of the MJO. As a follow-up report of the simulated MJO by Miura et al. (2007), Fudeyasu et al. (2008) presented the successful simulation of the complete life cycles of two real TCs, Bondo and Isobel, which formed over the Indian Ocean in the MJO experiment. Initialized with the atmospheric conditions two weeks before the genesis of Isobel, the model captured reasonably well not only the timing and motion but also the mesoscale structure and evolution of Isobel.

The main purpose of this study is to conduct a detailed analysis on the multiscale interactions involved in the life cycle of the simulated Isobel based on the output of the MJO experiment. This paper (Part I) focuses on the large-scale aspects of the genesis and subsequent storm-scale evolution. In a companion paper (Fudeyasu et al. 2010, hereinafter Part II), we will examine the involved mesoscale processes. The rest of the paper is organized as

follows. Section 2 briefly introduces the MJO experiment and the analysis methods. The simulated MJO and its associated westerly wind burst (WWB) and Tropical Storm Isobel are compared with those observed in section 3. The life cycle of the simulated Isobel is described in section 4. The evolution of the large-scale environmental conditions and the storm-scale structure change of the simulated Isobel are analyzed in section 5. The influence of the MJO on the life cycle of the simulated Isobel is further discussed in section 6. The major results are summarized in the last section.

2. The NICAM MJO experiment and analysis methods

NICAM has been developed at the Frontier Research Center for Global Change (FRCGC), at the Japan Agency for Marine Earth Science and Technology (JAMSTEC), and the Center for Climate System Research (CCSR), at the University of Tokyo, on the world's fastest-ever computer—the Earth Simulator in Japan. The model adopts the icosahedral horizontal grid system, which covers the globe quasi-homogeneously. The model physics include the explicit cloud microphysics scheme of Grabowski (1998) for moist processes, a simple bucket model for land surface processes, and the level-2 turbulence closure scheme of Nakanishi and Niino (2006) for subgrid-scale vertical mixing [see Tomita and Satoh (2004) and Satoh et al. (2008) for more details].

The MJO experiment used in this study was a 32-day simulation with realistic settings (the realistic initial conditions and terrain) and a horizontal resolution of about 7 km and 40 unevenly distributed vertical levels with the model top at about 38 km in a terrain-following height coordinate (Miura et al. 2007; Nasuno et al. 2009). The model was initialized at 0000 UTC 15 December 2006 with initial atmospheric variables and soil moisture from the National Centers for Environmental Prediction (NCEP) analysis, which has a horizontal resolution of 1.0° by 1.0°. The model provided outputs of 6-hourly snapshot three-dimensional variables and 1.5-hourly averaged two-dimensional variables.

The SST was spatially and temporally interpolated from the weekly Reynolds SST with a horizontal resolution of 1.0° by 1.0° (Reynolds and Smith 1994). Miura et al. (2008) performed two sensitivity experiments using the same model setting with the NICAM MJO experiment, but with a horizontal resolution of about 14 km. The time evolution of the simulated MJO event did not differ significantly between the simulations with the observed time-varying SST and the fixed climatological SST. The results implied that the simulated MJO was inherently an internal atmospheric mode and the observed SST was not critical to the eastward propagation of the MJO at least in the model for this case.

To facilitate our analysis of evolution of the large-scale circulation, we removed the TC signal from the model output using the smoothing algorithm developed by Kurihara et al. (1990). At first, the NICAM output was area averaged onto 1.0° by 1.0° grids. The disturbance field was filtered from the original field with successive applications of a simple smoothing operator. As a result, the basic fields consisting of only the large-scale circulation without either TC circulation or small-/mesoscale features were well retained, while waves having wavelengths less than 9° longitude–latitude were entirely removed from the original field and those with longer wavelengths were partially damped.

Definition of the TC center is critical to the calculation of the symmetric and asymmetric structures of the TC. Several methods were used to determine the storm center in this study. After 1800 UTC 28 December 2006 when Isobel had a clear signal in the sea level pressure (SLP) field, Isobel's center (xc, yc) was defined as the mass center (Wang 2007) given below

$$\mathrm{xc} = \frac{\int (p_r - p_s) x \, dx \, dy}{\int (p_r - p_s) \, dx \, dy}, \quad \mathrm{yc} = \frac{\int (p_r - p_s) y \, dx \, dy}{\int (p_r - p_s) \, dx \, dy}, \quad (1)$$

where p_s is the SLP and p_r is a reference pressure (here 1010 hPa). The integration domain is a circular area whose radius is approximately 210 km from the surface vortex center. Several iterations are required to get a converged solution because the integration radius depends on the storm center. Before 1800 UTC 28 December, the circulation center provides promising results. First, the wind field at each level was decomposed into basic field and disturbance field. The circulation center was defined as the center of the axisymmetric circulation along which the azimuthal-mean wind at 850 hPa reaches the maximum at a given time. Since the results using the circulation center at 850 hPa after 1800 UTC 28 December 2006 were essentially the same as that obtained based on the mass center, the 850-hPa circulation center was used to determine Isobel's center in the initial eddy stage (see section 4).

3. Verification of the simulation

a. The MJO and the associated WWB

Figure 1 shows the Hovmöller diagrams of anomalies in the observed blackbody temperature (T_{BB}) and the simulated outgoing longwave radiation (OLR) averaged between 15°N and 15°S. The observed T_{BB} was derived from the merged IR channels from five geostationary satellites of the Climate Prediction Center (CPC-IR).

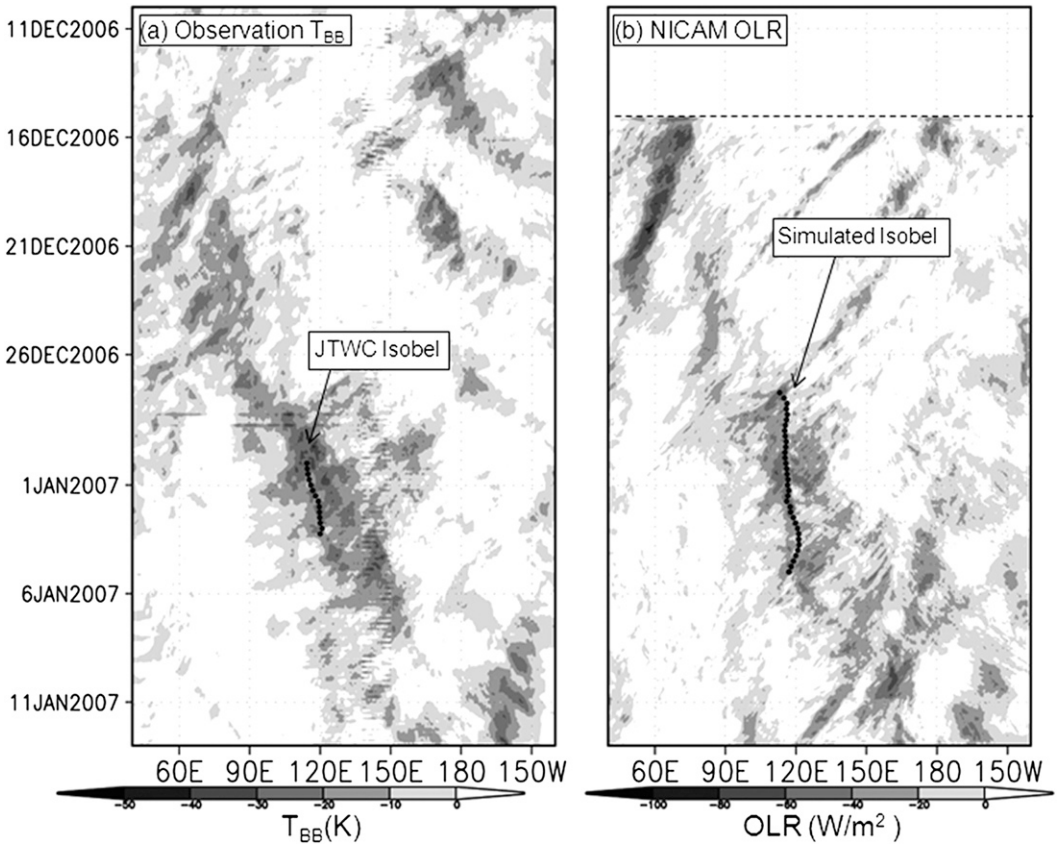

FIG. 1. Hovmöller diagrams of anomalies of (a) CPC-IR and (b) NICAM-OLR averaged between 15°N and 15°S. The anomalies are derived from the time average during 15 Dec 2006–15 Jan 2007. The solid line with filled circles represents Isobel's tracks from (a) JTWC and (b) NICAM.

The simulated OLR was area averaged onto a 0.25 grid to match the resolution of the satellite products. The evolution of the MJO event, characterized by an eastward propagation of the 5000–10 000-km convective envelope at approximately 5 m s^{-1} over 60°E–180°, was well reproduced in the model. However, compared with observations, the convective envelope in the simulation shifted 10°–20° longitude eastward over the East Indian Ocean and the Maritime Continent. Miura et al. (2007), Masunaga et al. (2008), Nasuno et al. (2009), and Liu et al. (2009) verified the evolution of this NICAM-simulated MJO event against various observations. They found that NICAM realistically simulated the three-dimensional structure of the MJO but the simulated MJO grew faster and had the amplitude larger than that observed.

Since the WWB associated with the MJO event is closely related to Isobel's life cycle, we briefly discuss the behavior of the WWB in both observation and simulation here. Although there are various definitions for the WWB (e.g., Murakami and Sumathipala 1989; Harrison and Vecchi 1997; Seiki and Takayabu 2007), we simply defined the WWB as the westerlies at 850 hPa greater than 1 m s^{-1} in the basic field associated with the MJO. To compare the evolution of the observed and simulated WWB quantitatively, we introduced the WWB front and WWB center. The former was defined by the eastern boundary (easternmost point) of the WWB, while the latter was the location of the maximum westerly in the WWB.

Figure 2 shows the evolution of the WWB in the NCEP analysis and the NICAM simulation. In NICAM, the WWB front and center started to appear over the East Indian Ocean on 24 December and moved eastward toward the western Pacific (Figs. 2b,d). The real WWB also started to appear on 24 December but the location of the WWB front and center were 10°–20° longitude west of those simulated (Figs. 2a,c). As a result, the WWB in the simulation arrived at the Maritime Continent about two days earlier. After the passage of the WWB front over the Java Sea, both the observed and simulated MJO continued to move eastward but the simulated front shifted 10°–15° latitude southward away from the equator. The intensity of the simulated WWB showed an evolution similar to that observed but about 30% stronger (Fig. 2e). This is consistent with the analysis by Liu et al. (2009), who

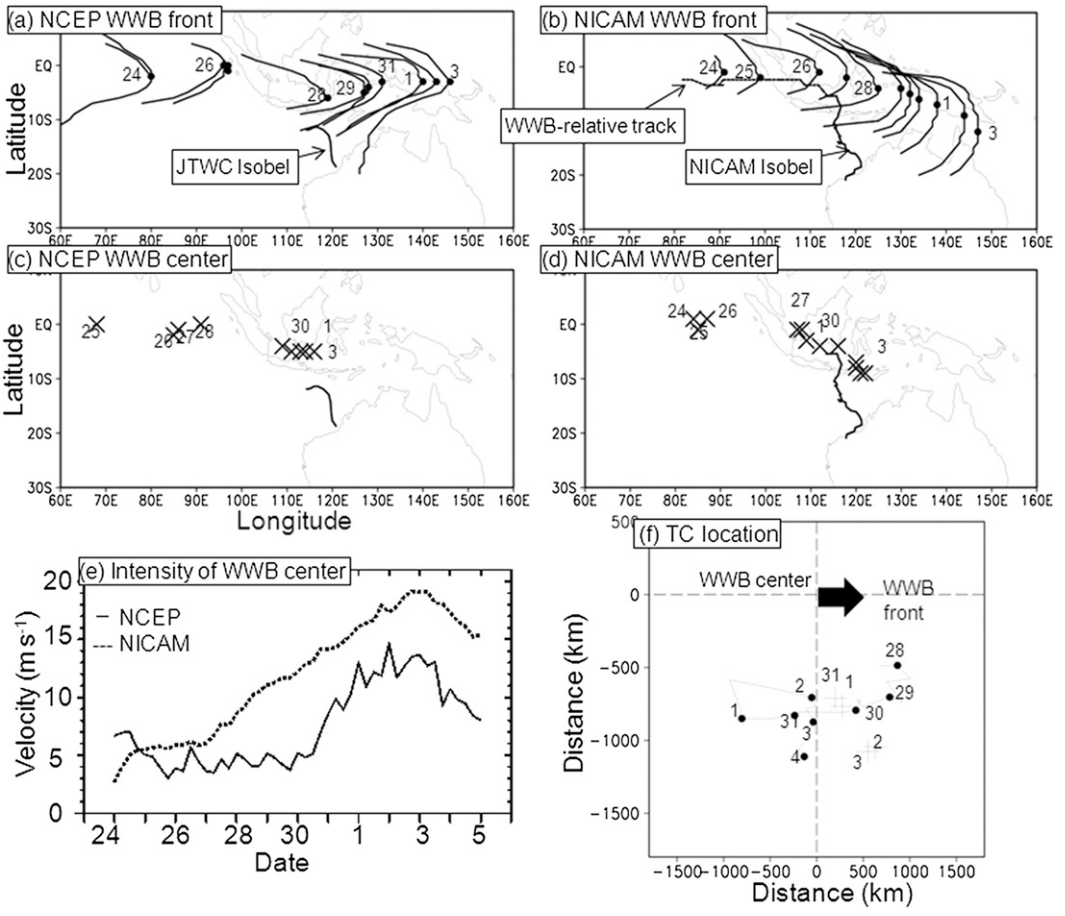

FIG. 2. Temporal evolution of (a),(b) the WWB front (solid line) and front point (closed circle) and (c),(d) the WWB center at 0000 UTC derived from (a),(c) the NCEP analysis and (b),(d) the NICAM simulation. Solid lines represent (a),(c) the JTWC and (b),(d) the simulated Isobel's tracks. The dotted line in (b) represents the track relative to the WWB front point. (e) Temporal evolution of the WWB intensity derived from the NCEP analysis (solid) and the NICAM simulation (dot) and (f) the location of Isobel relative to the WWB center. Tracks and locations at 0000 UTC (solid line and closed circle) from the simulated Isobel are compared with those from the JTWC best track (cross). Numbers mean the dates of the month.

showed that the simulated MJO event grew faster over the Indian Ocean and the Maritime Continent and had an intensity about 30% stronger than the observed. We will show in section 3b that biases in the simulated MJO were responsible for the discrepancies in the life cycle of the simulated Isobel.

b. An overview of the observed and simulated Isobel

The genesis of Isobel was associated with the onset of the MJO over the East Indian Ocean in both simulation and observation. The observed Isobel was located to the southeast of the WWB center based on the Joint Typhoon Warning Center (JTWC) best-track data (Fig. 2f). Similar to the genesis of the observed Isobel, the simulated Isobel formed in the southeast quadrant of the WWB about 700 km from the WWB center. According to the best-track data from both JTWC and the Australian Bureau of Meteorology (BoM), the actual Isobel was first detected over the Timor Sea south of the Java Island on 31 December 2006 (Fig. 3a). The track of the simulated Isobel was very close to that observed from 31 December.

The central SLP of the observed Isobel remained steady around 1000 hPa for 2 days after its formation according to the JTWC and BoM best-track data (Fig. 3b) and then deepened and reached the minimum of 994 hPa at 1800 UTC 2 January by JTWC and 980 hPa at 1200 UTC 2 January by BoM. [Postanalysis of Isobel by BoM indicated that the circulation did not reach tropical cyclone intensity (see online at http://www.bom.gov.au/weather/wa/cyclone/about/seasonsummary200607.shtml). On the other hand, the JTWC final report (available online at http://metocph.nmci.navy.mil/jtwc/atcr/2007atcr/2007atcr.pdf) indicated that Isobel reached the tropical storm intensity. Our focus in this study is to understand the multiscale

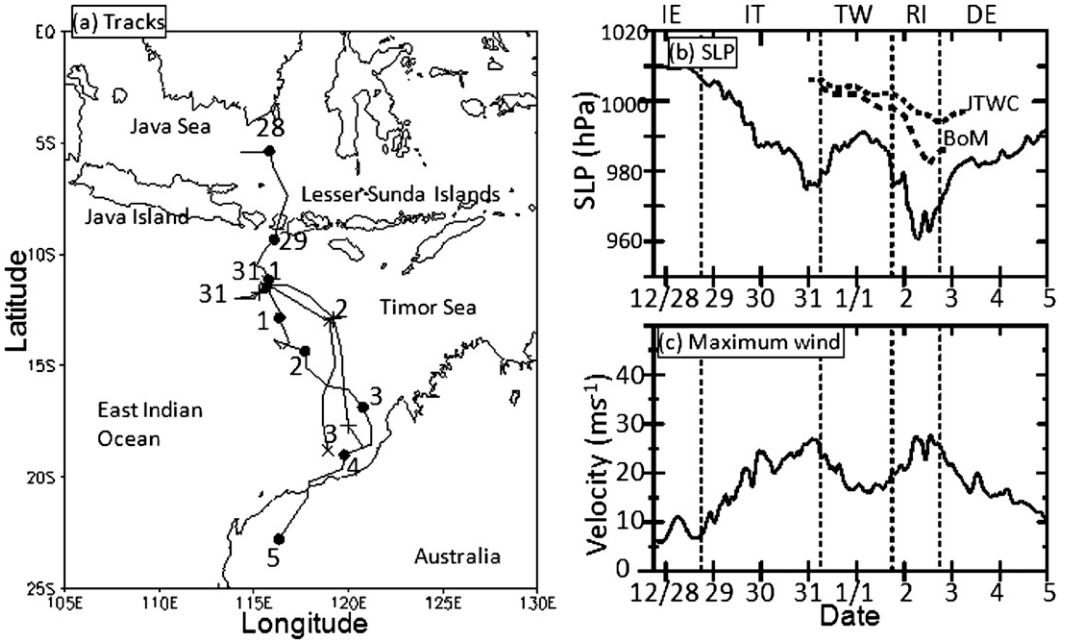

FIG. 3. (a) Tracks and locations at 0000 UTC (line and closed circle) from the simulated Isobel, compared with those from the BoM best-track (line and cross) and the JTWC best-track (line and plus). Numbers mean the dates of the month. (b) Temporal evolution of the central SLP (hPa) from the NICAM simulation (solid) and BoM and JTWC best tracks (dashed). (c) Temporal evolution of the simulated maximum azimuthal-mean surface wind speed (m s^{-1}).

interactions involved in the simulated Isobel. Therefore, the difference in the storm intensity from the observation is not the key.] The central SLP of the simulated Isobel was about 10 and 35 hPa deeper than that of JTWC and BoM, respectively. This discrepancy could be attributed to the simulated too strong WWB in the model. Nevertheless, the model reproduced the stagnant nature of the movement during the first 2 days and the subsequent intensification and weakening of the observed Isobel (Figs. 3a,b).

Figure 4 shows the hourly rainfall rate derived from the Tropical Rainfall Measuring Mission (TRMM) Microwave Imager (TMI) and the Quick Scatterometer (QuikSCAT) sea surface winds (Freilich and Dunbar 1999; Chelton and Freilich 2005). Prior to the first detection of Isobel by JTWC and BoM, there were regions with organized convection associated with the MJO and its WWB around the Java Island on 30 December 2006. The zonally elongated rainband labeled A in Fig. 4 was organized over the Java Sea at 1200 UTC 30 December 2006. The rainband A moved southeastward and entered the Timor Sea on 1 January 2007 and evolved into cloud clusters. Another rainfall region, labeled B in Fig. 4, was organized over the Timor Sea south of the Java Island on 31 December. BoM and JTWC first detected the center of Isobel near the cloud cluster B on 31 December. On 1 January 2007, the cluster B weakened over the Timor Sea. The detected center of Isobel was between clusters A and B, as seen from the circulation center in the surface wind field on 1 January 2007. The two clusters merged to the north of the circulation center over the Timor Sea at 0000 UTC 2 January and subsequently became the spiral rainband and the partial eyewall of Isobel.

A similar rainband formed over the Java Sea in the simulation was about two days too early (Fig. 5) compared with that in the observations (Fig. 4). This was primarily due to the too early growth of the WWB and the associated convection over the Maritime Continent in the simulation (Figs. 1 and 2). Nevertheless, although the details are somewhat different, the overall rainfall features of the simulated Isobel are comparable to those observed (Figs. 4 and 5), including the asymmetric rainfall distribution in the inner-core region. The spiral rainband southwest of actual Isobel's center at 0000 UTC 2 January (Fig. 4) also appeared in the simulation between 1800 UTC 1 January and 0000 UTC 2 January (Fig. 5). As Isobel was approaching the northwest coast of Australia after 0000 UTC 3 January, intense rainfall occurred over the land south of Isobel's center (Fig. 4). This asymmetric rainfall pattern between 1200 UTC 3 January and 0000 UTC 4 January was also reproduced by the model (Fig. 5).

Note that although the early formation stage of the simulated Isobel was not compared well with that in the BoM or JTWC best-track data, satellite observations showed the linkage between the cloud/rainfall pattern organized in the MJO over the Java Sea and the genesis of

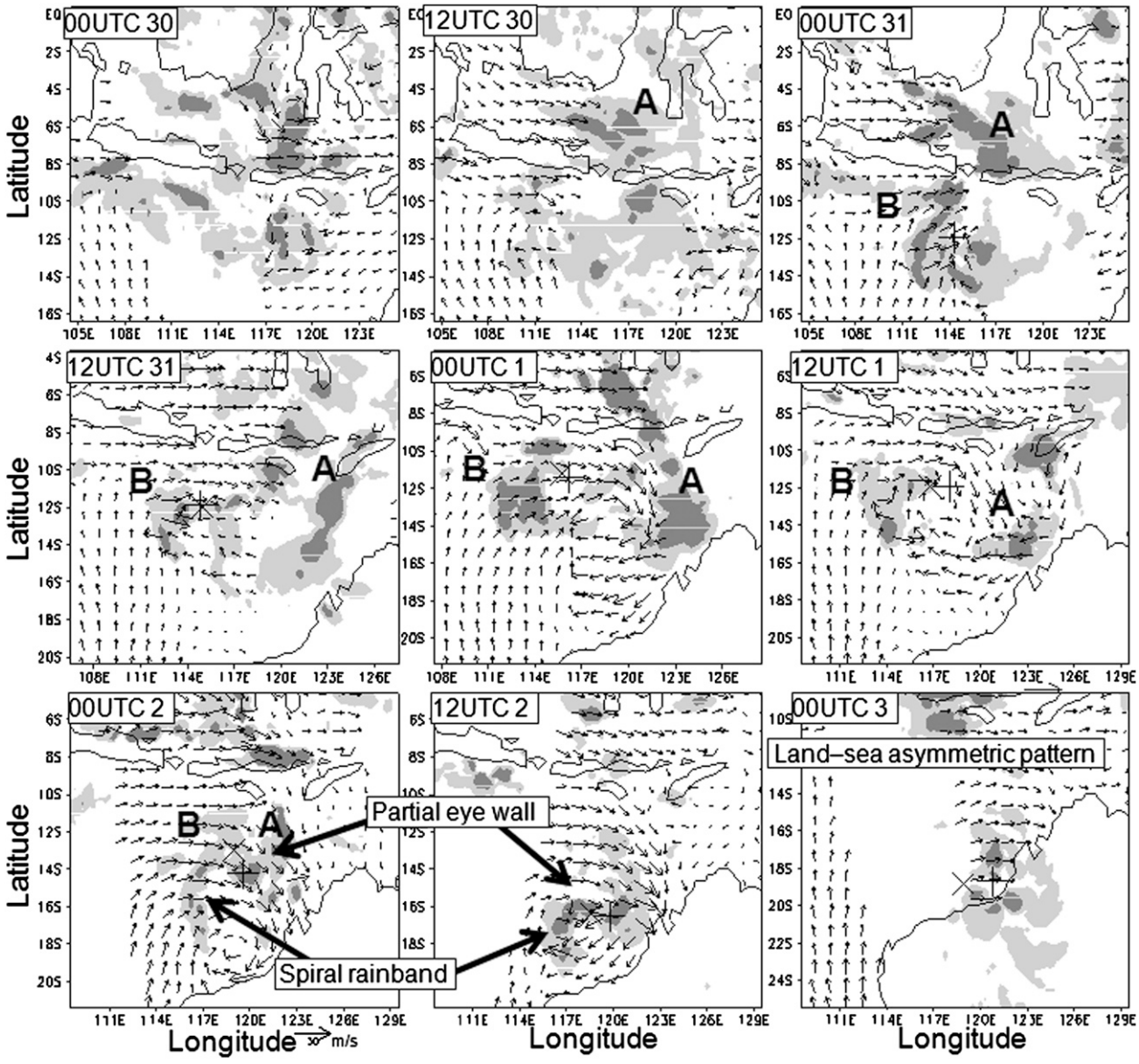

FIG. 4. Rainfall rate (mm h^{-1}, shaded) derived from the TRMM TMI and surface wind (m s^{-1}) measured by NASA's Quick Scatterometer. Light (dark) shading represents areas with rainfall rate larger than 0.5 mm h^{-1} (5 mm h^{-1}). The crosses and pluses from 31 Dec 2006 to 3 Jan 2007 represent the cyclone center derived from the BoM and JTWC best track, respectively.

Isobel. This linkage was well simulated in NICAM as will be discussed in the next sections. Therefore, the MJO experiment captured reasonably well the life cycle of Isobel as already shown in Fudeyasu et al. (2008). This allows us to further understand the multiscale interactions in Isobel's life cycle based on the NICAM simulation in this study.

4. The life cycle of the simulated Isobel

To facilitate the discussion, we divided the life cycle of the simulated Isobel into five stages (Table 1). We refer to the period from 1800 UTC 27 December to 1800 UTC 28 December 2006, prior to Isobel being detectable in SLP field, as the initial eddy stage. At 1800 UTC 27 December, convective cyclonic eddies appeared in a zonally oriented rainband over the Java Sea (see Part II). These eddies moved southeastward over the Java Sea and made landfall on one of the Lesser Sunda Islands at 1800 UTC 28 December. The surface relative cyclonic vorticity averaged within a radius of 50 km from the initial eddy's center first increased and then decreased slightly (Fig. 6a) as the eddies approached the Lesser Sunda Islands (Fig. 3a). The maximum azimuthal-mean surface wind speed increased (Fig. 3c) and the radius of maximum wind

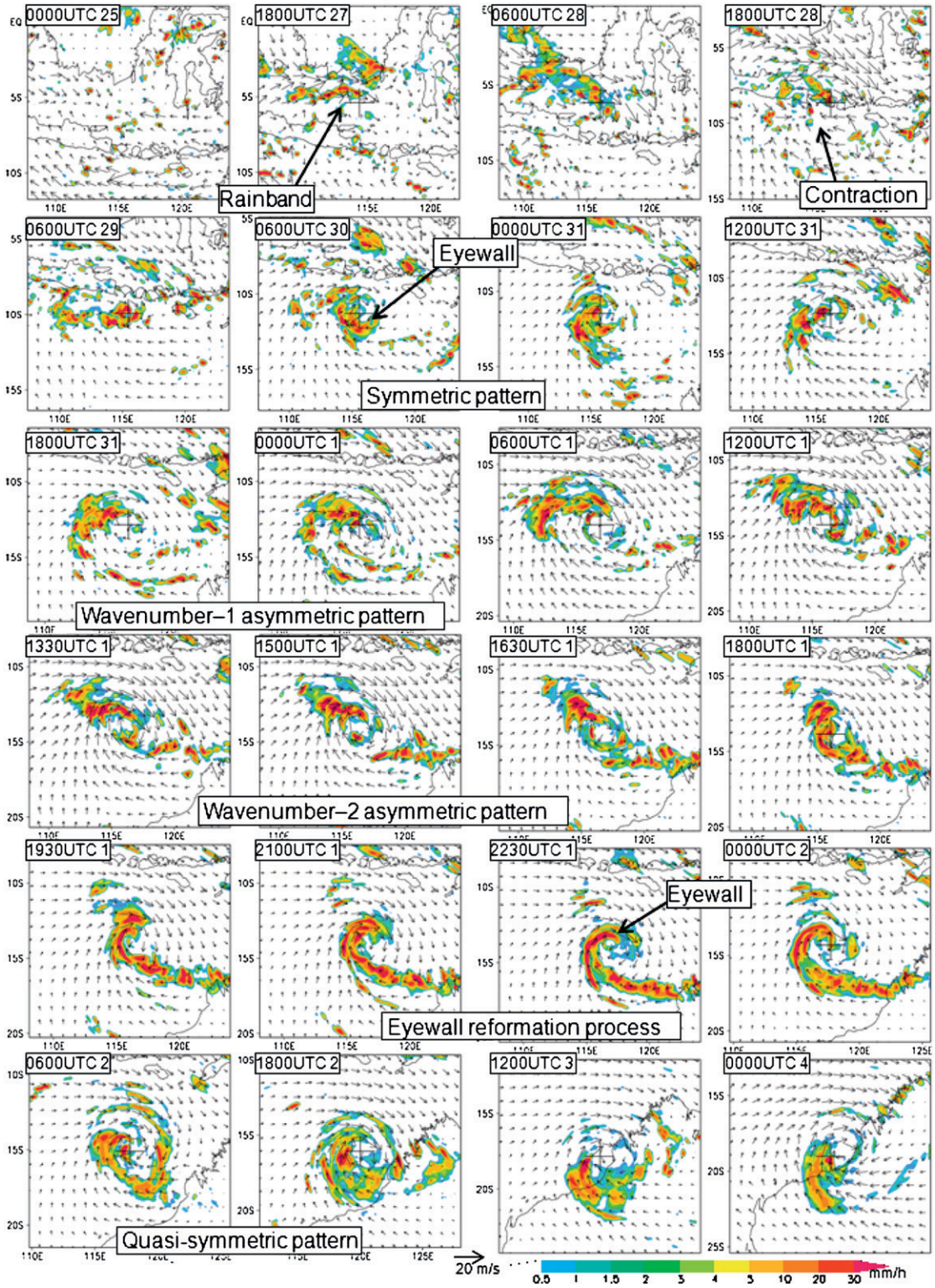

FIG. 5. Rainfall rate (mm h^{-1}, shaded) and surface (10-m height) winds (m s^{-1}) from the NICAM simulation. The crosses represent Isobel's center.

TABLE 1. List of different stages in the simulated Isobel's life cycle and characteristics of the storm evolution, rainfall pattern, large-scale setting, and the dominant effects: minimum surface pressure (SP), mid–upper troposphere (UL), vertical shear (VS), TC-scale vorticity (TC), low-level horizontal cyclonic shear (CS), steering flow (layer mean flow) (SF), inner core convection (eyewall) (EW), low-level horizontal convergence (CO), low-level stretching deformation (SD), large-scale velocity (CV), low-level zonal divergence (ZD), and wavenumber (WN).

Life stage (abbreviation)	Period	Characteristics			
		TC evolution	Rainfall	Large-scale setting	Dominant effects
Preconditioning (PC)	0000 UTC 27 Dec–1800 UTC 27 Dec 2006	No detection	Rainband formation	MJO onset	Strong CO/CV/VS High CAPE
Initial eddy (IE)	1800 UTC 27 Dec–1800 UTC 28 Dec 2006	IE genesis No SP signal	Contraction	Enhanced WWB	Strong CO/CV Strong VS/SF
Intensifying (IN)	1800 UTC 28 Dec–0600 UTC 31 Dec 2006	TC developing SP decreasing	EW formation	Easterly trade winds Weak UL winds	Strong CS/CV Weak VS/SF
Temporary weakening (TW)	0600 UTC 31 Dec 2006–1800 UTC 1 Jan 2007	TC weakening SP increasing	EW breakdown		
Early TW	0600 UTC 31 Dec 2006–0600 UTC 1 Jan 2007		WN-1 asymmetry	Strong UL easterly	Strong VS
Late TW	0600–1800 UTC 1 Jan 2007		WN-2 asymmetry	Shift of WWB center	Positive SD/ZD
Reintensifying (RI)	1800 UTC 1 Jan–1800 UTC 2 Jan 2007	TC developing SP minimum	EW reformation	Enhanced WWB	Change in VS Strong SF
Decaying (DE)	1800 UTC 2 Jan–0000 UTC 5 Jan 2007	TC weakening SP increasing	EW breakdown	Strong UL northerly	Strong VS/SF Landfall effect

(RMW) decreased (Fig. 6b). Rainfall averaged within a radius of about 50 km increased whereas that averaged within a radius of 100 km changed little and that averaged between radii of 100 and 200 km decreased (Fig. 6c), indicating a contraction of the rainfall region (Fig. 5).

The initial eddy stage was followed by a period during which Isobel's central SLP decreased to the first minimum of about 975 hPa at 0000 UTC 31 December (Fig. 3b). The period from 1800 UTC 28 December to 0600 UTC 31 December is thus referred to as the intensifying stage (Table 1). During this period, both the maximum surface wind speed and the surface cyclonic relative vorticity averaged within a radius of 50 km increased rapidly (Figs. 3c and 6a), while the RMW remained between 30 and 40 km (Fig. 6b). The rainfall increased in the outer region (Fig. 6c). A distinct feature at this stage is the increase in the radius of the azimuthal-mean 15 m s^{-1} surface wind (Fig. 6b), indicating the development of the storm-scale circulation. Isobel showed little movement over the Timor Sea during the intensifying stage (Fig. 3a).

The intensification of the simulated Isobel was interrupted at around 0600 UTC 31 December and the storm weakened until 1800 UTC 1 January 2007 with the central SLP increased by 15 to 990 hPa (Fig. 3b). This period is referred to as the temporary weakening stage (Table 1). The maximum surface wind speed decreased by about 15 m s^{-1} (Fig. 3c) and the increase in the surface cyclonic relative vorticity slowed down considerably (Fig. 6a). Rainfall showed a significant decrease, in particular, within a radius of 50 km (Fig. 6c), indicating a weakening of the inner-core convection. The simulated Isobel showed an unusual track with a cyclonic rotation over the Timor Sea during the late temporary weakening stage (Fig. 3a).

The simulated Isobel started to reintensify from 1800 UTC 1 January, referred to as the reintensifying stage (Table 1). Its central SLP decreased and reached its lifetime minimum value of about 960 hPa at 0600 UTC 2 January (Fig. 3b). The maximum azimuthal-mean surface wind speed increased by about 25 m s^{-1} (Fig. 3c) and the surface relative vorticity averaged within a radius of 50 km reached the lifetime minimum value of about -4×10^{-4} s^{-1} (Fig. 6a). By the end of the reintensifying stage, Isobel headed southeastward toward the northwest coast of Australia and started to weaken (Figs. 3 and 6), namely, the decaying stage of the simulated Isobel. Both the central SLP and the surface relative vorticity increased rapidly (Figs. 3b and 6a). The maximum surface wind speed decreased with an increase in the RMW (Figs. 3c and 6b). Isobel made landfall at 1200 UTC 4 January with its central SLP of about 990 hPa (Fig. 3a). Therefore, the MJO experiment simulated the week-long life cycle of Isobel comparable to the typical life cycle of a TC (Wang and Wu 2004).

5. Evolution of the large-scale circulation and storm-scale structure change

a. Preconditioning of the genesis and intensification of Isobel

Figure 7 shows the large-scale basic winds at 850, 500, and 200 hPa from 1800 UTC 27 December 2006 to 1200 UTC 2 January 2007. On 27–28 December, the WWB developed over the East Indian Ocean and the Java Sea

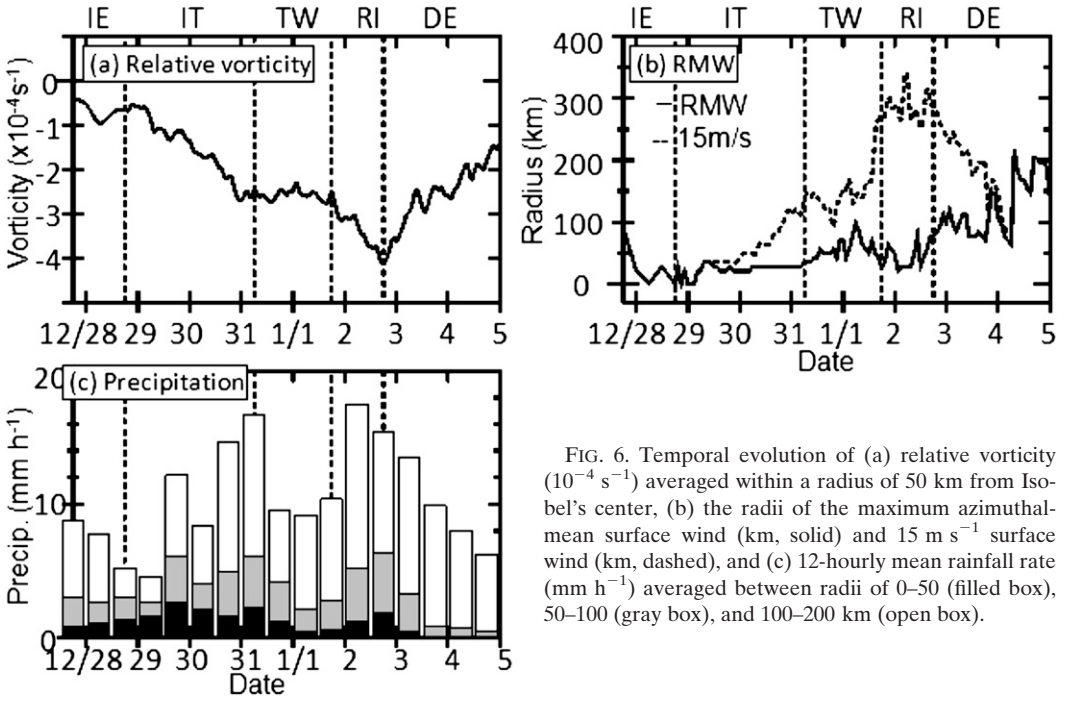

FIG. 6. Temporal evolution of (a) relative vorticity (10^{-4} s^{-1}) averaged within a radius of 50 km from Isobel's center, (b) the radii of the maximum azimuthal-mean surface wind (km, solid) and 15 m s^{-1} surface wind (km, dashed), and (c) 12-hourly mean rainfall rate (mm h^{-1}) averaged between radii of 0–50 (filled box), 50–100 (gray box), and 100–200 km (open box).

associated with the onset of the MJO (Fig. 7a). The low-level WWB extended east-southeastward during 29–30 December, while the easterly trade winds extended westward around the latitude of 15°S south of Isobel (Fig. 7b). The upper troposphere was dominated by easterlies in the equatorial region and westerlies to the south in the midlatitude.

The evolution of several large-scale parameters derived from the basic wind field and averaged within a radius of 500 km from Isobel's center is shown in Fig. 8. Note that before the initial eddy stage Isobel's center was fixed at the center of the initial eddies over the Java Sea at 1800 UTC 27 December (also in Figs. 9–13). The low-level cyclonic shear and convergence of zonal wind (du/dy and du/dx) increased over the Java Sea from 27 December, providing a favorable large-scale condition for the organization of small-/mesoscale convective vortices (Figs. 8a,b). In the following days, the low-level large-scale cyclonic shear around Isobel was enhanced by the WWB and easterly trade winds over the Timor Sea (Fig. 7b). The convective available potential energy (CAPE) following Isobel's center was high (>500 J kg^{-1}) over the Maritime Continent before 27 December, while it decreased afterward as a result of enhanced convection associated with the WWB over the Java Sea during the initial eddy stage (Fig. 8d).

For a comparison, Fig. 8 also shows the averaging following the MJO during 24–28 December 2006 (labeled MJO in Fig. 8). The centers of the average were determined based on the position of Isobel relative to the eastward-propagating WWB front, as shown in Fig. 2b. Namely, the average regions were located in the Indian Ocean during 24–25 December, while in the Java Sea during 26–28 December. The average region relative to the MJO front was always accompanied with strong horizontal cyclonic shear and convergence of zonal wind (du/dx and du/dy) and strong vertical shear (Figs. 8a,c), whereas convergence/shear of meridional wind (dv/dx and dv/dy) were negligible (not shown). The CAPE increased with time as the MJO moved toward the Maritime Continent (Fig. 8d). Therefore, the preconditioned large-scale environment set high CAPE around the Maritime Continent, and low-level cyclonic vorticity and convergence over the Java Sea, leading to active convection and the genesis of Isobel.

Figure 9 shows the time–latitude (time–longitude) cross section of zonal winds of the basic flow zonally (meridionally) averaged within 500 km from the longitude (latitude) of Isobel's center at 850 hPa. The WWB associated with the MJO appeared in the equatorial region on 26 December 2006 and extended southward gradually, reaching the Java Sea at around 6°S at 0000 UTC 27 December. The initial eddies formed southeast of the maximum low-level westerlies in the WWB at 1800 UTC 27 December (Figs. 2f and 9). The westerlies continued to extend southeastward and reached the Lesser Sunda Islands by 29 December. Isobel formed and developed in the westerly slightly north of the cyclonic shear line (0 m s^{-1} of averaged zonal winds) in the lower troposphere.

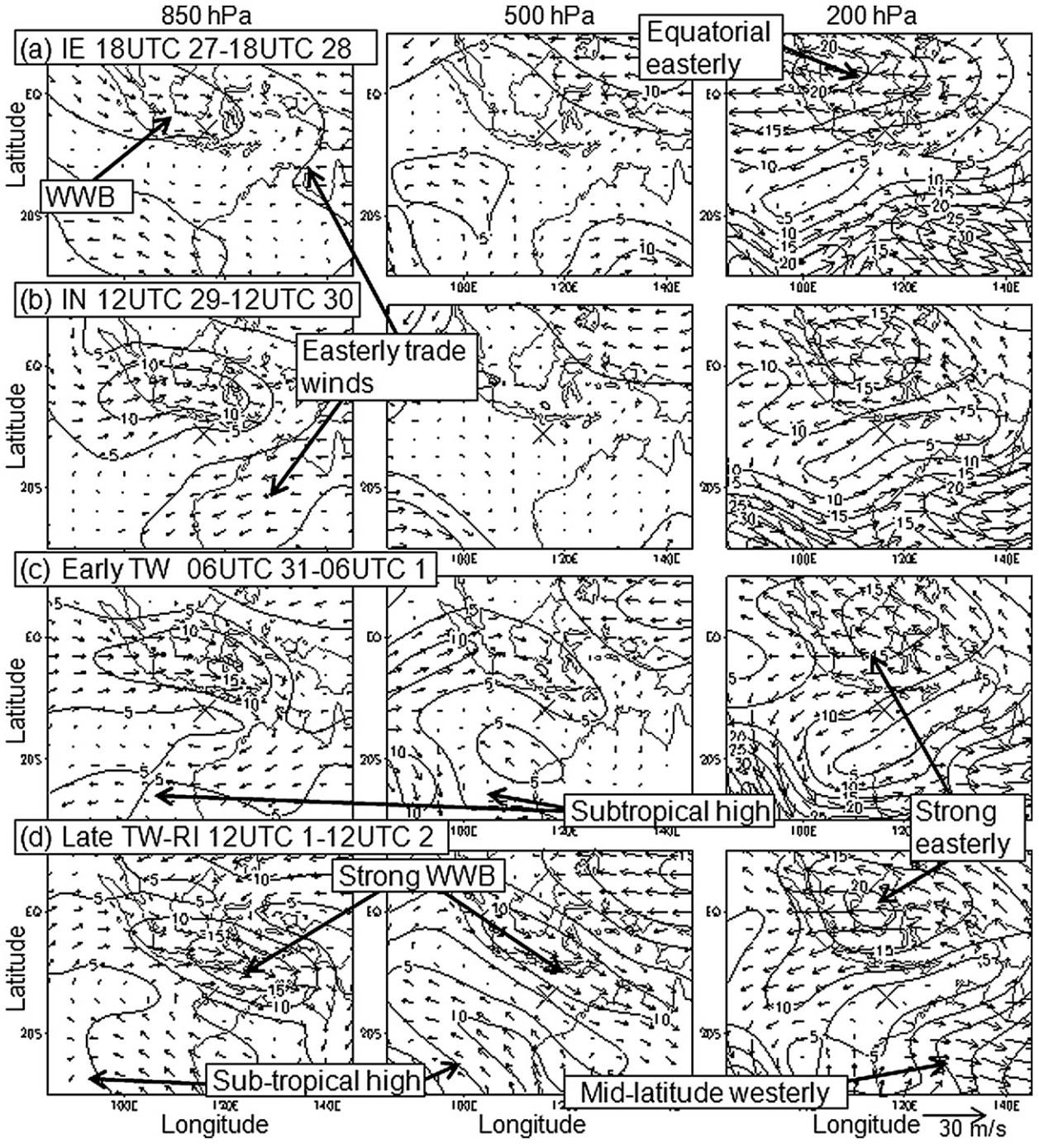

FIG. 7. The horizontal wind (m s^{-1}) and wind velocity (m s^{-1}, contour) of the basic fields of (left) 850-, (middle) 500-, and (right) 200-hPa 24-hourly mean started at (a) 1800 UTC 27 Dec, (b) 1200 UTC 29 Dec, (c) 0600 UTC 31 Dec 2006, and (d) 1200 UTC 1 Jan 2007. The contour interval is 5 m s^{-1}. The cross represents the storm center at the starting time of the averaged period.

Figure 10 shows the time–height cross section of the basic wind field averaged within a radius of 500 km from the storm center with vectors showing the vertical shear, Isobel's motion, and deep/shallow layer mean flow. From 26 December, the easterly vertical shear increased rapidly (Figs. 8c and 10), which resulted from the development of the low-level westerlies associated with the WWB. As the initial eddies moved southward away from the region of the equatorial upper-level easterlies, the vertical shear decreased during both the late initial eddy stage and the early intensifying stage (Figs. 7b, 8c, and 10). The development of Isobel benefited from the enhanced

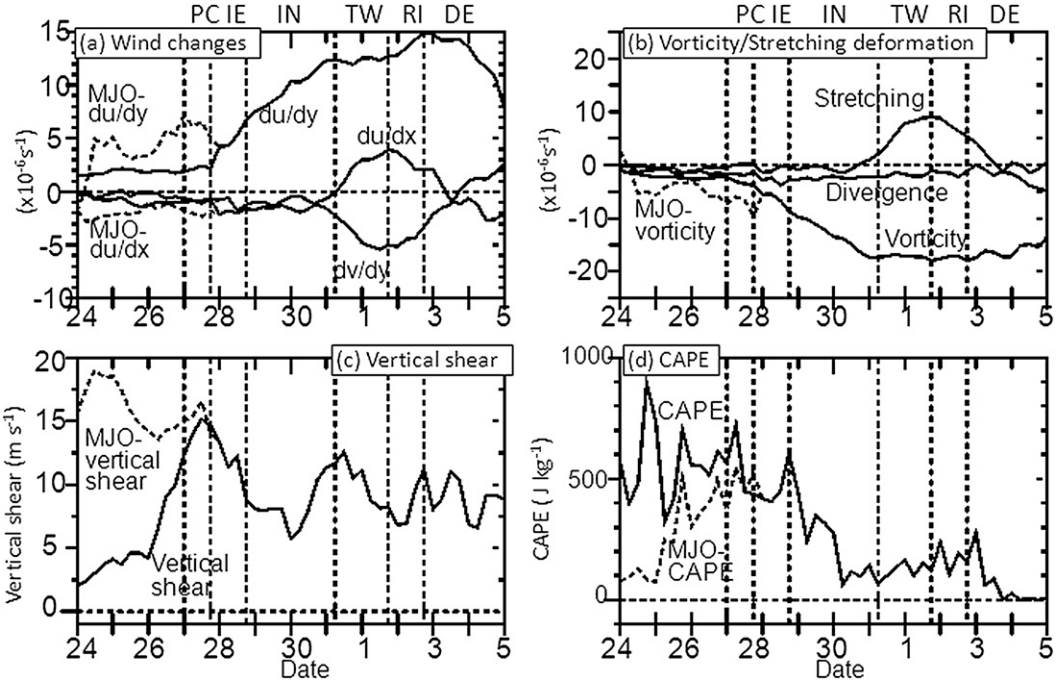

FIG. 8. Temporal evolution of (a) zonal divergence (10^{-6} s^{-1}, du/dx, solid), zonal shear (10^{-6} s^{-1}, du/dy, solid), and meridional divergence (10^{-6} s^{-1}, dv/dy, solid) at 850 hPa; (b) relative vorticity (10^{-6} s^{-1}, solid), divergence (10^{-6} s^{-1}, solid), and horizontal stretching deformation (10^{-6} s^{-1}, solid) at 850 hPa; (c) vertical shear (m s^{-1}, solid) between 200 and 850 hPa; and (d) CAPE (J kg^{-1}, solid) in the basic fields averaged within a radius of 500 km from Isobel's center. The location of Isobel's center is fixed at the center of the initial eddies at 1800 UTC 27 Dec during 0000 UTC 24 Dec–1800 UTC 27 Dec. Results for the average region moved following the WWB front with Isobel's center relative to the WWB front point at 0000 UTC 28 Dec as the reference shown in Fig. 2b are displayed as a dashed line (labeled MJO).

low-level large-scale cyclonic vorticity and weak vertical shear over the Timor Sea in the intensifying stage. The mid–upper-level winds were relatively weak around Isobel (Figs. 7b and 10), consistent with the weak steering flow and little movement of Isobel (Fig. 3a).

The vertical profiles of relative vorticity averaged within a radius of 301 km from Isobel's center and potential temperature anomaly averaged within a radius of 49 km are shown in Fig. 11. The cyclonic vorticity started to develop below about 4 km at 1800 UTC 27 December, a signal of the genesis of initial eddies. After their geneses, the initial eddies moved eastward until 0600 UTC 28 December and then southward until 0000 UTC 29 December (Fig. 3a). At the end of the initial eddy stage, the cyclonic vorticity developed upward into the upper troposphere (Fig. 11a). The warm anomaly formed in the upper troposphere in the inner core with the maximum temperature anomaly at about 9–12 km (Fig. 11b). This was accompanied by a decrease in Isobel's central SLP (Fig. 3b), indicating that Isobel developed a TC structure.

The azimuthal-mean rainfall rate shows a contraction of the rainfall region in the initial eddy stage (Fig. 12), which indicates an intensification of the initial eddies. This is consistent with the findings of Zehr (1992), who noted the inward contraction of convection during the TC genesis from observations. On 30 December in the late intensifying stage, the azimuthal-mean heavy rainfall occurred between radii of 20 and 40 km with little rainfall within 20 km, a sign of the formation of an eye and eyewall. By 1800 UTC 30 December, a rainband developed about 50 km to the west of Isobel's center and propagated radially outward (Fig. 5).

By the end of the initial eddy stage, the circulation center tilted westward with height, and in the late initial eddy and early intensifying stages the upper-level centers coincided with the mid- and low-level centers (not shown), indicating that Isobel developed a vertically aligned deep circulation. Figure 13a shows the ''axisymmetricity'' defined as

$$\text{axisymmetricity}(\%) = \left(1 - \frac{\int_0^{r=301\text{km}} \text{EKE}\, dr}{\int_0^{r=301} \text{KE}\, dr}\right) \times 100, \quad (2)$$

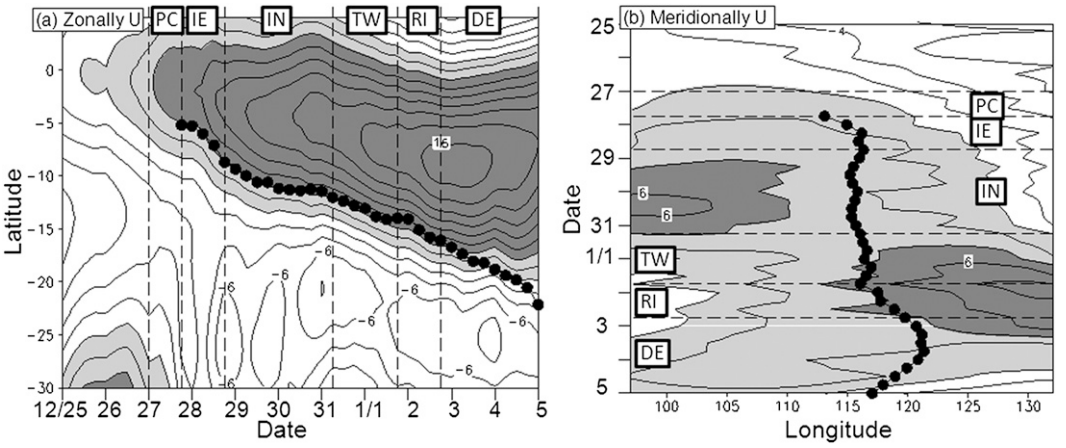

FIG. 9. (a) The time–latitude cross section of the 850-hPa zonal wind (m s^{-1}) of the basic field zonally averaged within 500 km from the longitude of Isobel's center and (b) the time–longitude cross section of the 850-hPa zonal wind of the basic field meridionally averaged within 500 km from the latitude of Isobel's center. The contour interval is 2 m s^{-1}. Light shading represents westerlies and dark shading represents areas of westerlies stronger than 4 m s^{-1}. The solid line with closed circles represents Isobel's track.

where KE is the azimuthal-mean kinetic energy, EKE is the azimuthal-mean eddy kinetic energy (Wang 2007, 2008), and r is the radius from the storm center. The axisymmetricity was quite small in the early initial eddy stage while it increased in the late initial and intensifying stages. The development of symmetric structure with vertically aligned deep circulation of Isobel was consistent with the favorable environment with a weak vertical shear.

b. *Unfavorable large-scale circulation and the interruption of intensification*

The cyclonic vorticity of Isobel decreased in the mid–upper troposphere during the temporary weakening stage, which was accompanied by a weakening of the warm core in the upper troposphere and an increase in the central SLP (Figs. 3b and 11). Convection in the inner core was suppressed whereas convection outside the inner core only weakened slightly during the temporary weakening stage (Fig. 12). These structural changes were consistent with the negative effect of the large-scale circulation, which was characterized by strong vertical shear in the early temporary weakening stage and then a strong horizontal stretching deformation field in the late temporary weakening stage. From 31 December 2006 to 1 January 2007, upper-level easterlies strengthened around Isobel (Fig. 7c), leading to an increase in easterly vertical shear (Figs. 8c and 10). Corresponding to the strong easterly shear, the upper-level circulation centers of Isobel shifted westward from the mid–lower-level centers (not shown) with deep convection enhanced downshear (Fig. 5), consistent with previous studies (Wang and Holland 1996; Frank and Ritchie 1999).

The axisymmetricity decreased in the temporary weakening stage (Fig. 13a). The asymmetry was dominated by the wavenumber-1 component in the mid–upper troposphere in the late intensifying and early temporary weakening stages (Figs. 13b,c), which can be explained by the influence of the strong vertical shear. From 1200 UTC 1 January, Isobel moved to the region with weak upper-tropospheric winds between strong easterlies to the north and midlatitude westerlies to the south (Fig. 7d). As a result, the vertical shear decreased (Figs. 8c and 10) and the westward vertical tilt of the storm center was reduced in the late temporary weakening stage (not shown).

Isobel remained in the westerlies in the lower troposphere during the intensifying and the temporarily weakening stages (Fig. 9). The WWB moved southeastward and the WWB center shifted to the east of Isobel (Figs. 2f, 7d, and 9b), leading to the low-level divergence of zonal wind (du/dx) around Isobel (Fig. 8a). In contrast, its meridional convergence (dv/dy) between the southerlies east of the subtropical high developed over the East Indian Ocean and the northerlies of the southeastwardly extended WWB increased around Isobel. These mid–lower-tropospheric zonal divergence and meridional convergence contribute to an increase in the large-scale stretching deformation field (Fig. 8b). The axisymmetricity remained small in the late temporary weakening stage. Although the total asymmetry was still dominated by a wavenumber-1 asymmetry (Figs. 13b,c), a wavenumber-2 asymmetry appeared in the mid–lower troposphere in the late temporary weakening stage (Fig. 13d) when the large-scale stretching deformation field was strong. During 1200–1800 UTC 1 January, the rainfall rate in Isobel showed two spiral rainbands (Fig. 5), indicating the development of

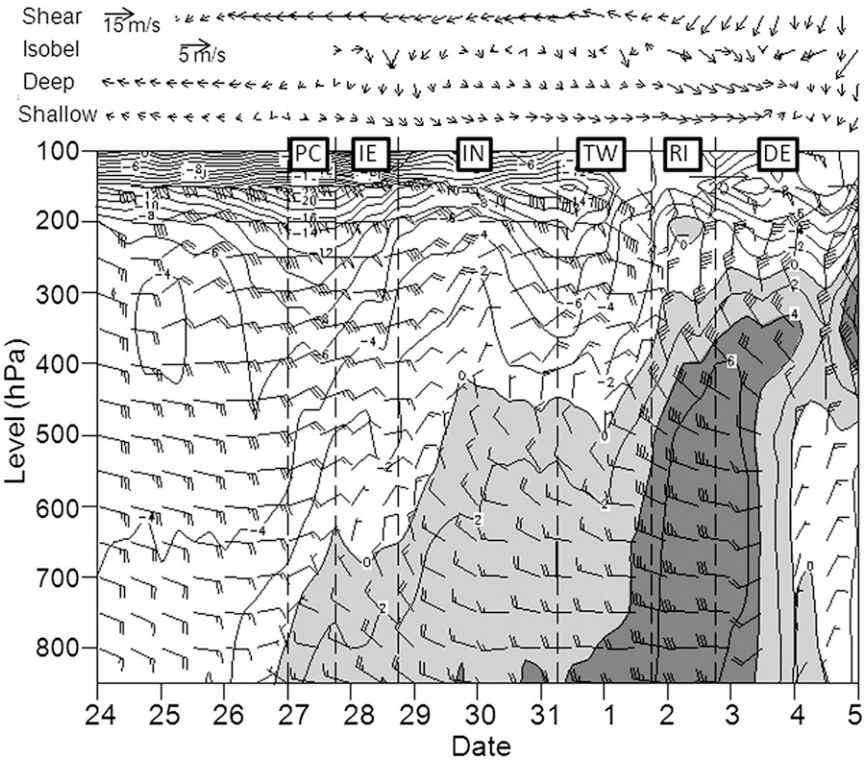

FIG. 10. Time–height cross section of horizontal winds (m s^{-1}, barb) of the basic flow averaged within a radius of 500 km from Isobel's center. The contour interval is 2 m s^{-1} of zonal wind. Light shading represents westerlies and dark shading represents zonal wind stronger than 4 m s^{-1}. Full wind barb represents 10 m s^{-1}. The vectors above show the vertical shear vector, Isobel's motion, and the deep-layer (850–300 hPa) and shallow-layer (850–700 hPa) mean winds derived from the basic wind field within a radius of 500 km.

a wavenumber-2 asymmetry in Isobel in the strong stretching deformation field.

c. *Changes in large-scale circulation and reintensification of Isobel*

During 1–2 January 2007, the WWB extended southeastward and strengthened in the lower troposphere, causing the appearance of northwesterlies in the midtroposphere over the Java Sea and the eastern Timor Sea (Fig. 7d). The midlevel northwesterlies resulted in a fast southeastward movement of Isobel (Figs. 3a and 10). The vertical shear over Isobel changed from easterly shear to north-northeasterly shear accordingly (Fig. 10). The cyclonic vorticity of Isobel developed again throughout the troposphere at the beginning of the reintensifying stage with the warm core in the upper troposphere strengthened (Fig. 11) and Isobel reintensified (Figs. 3b,c).

The reintensification of Isobel was associated with the eyewall reformation through the axisymmetrization of an inward-propagating outer spiral rainband (Figs. 5 and 13a). At 1500 UTC 1 January, the eyewall convection showed some discrete cloud features. A large outer spiral rainband was initiated to the southeast of Isobel's center at around 15°–16°S, downwind of the strengthened WWB center. The rainband was enhanced by an intense confluence zone between the strong northwesterlies of the WWB and southeasterly trade winds at 1800 UTC 1 January (Figs. 5 and 7d). By 2100 UTC 1 January, the spiral rainband continuously enhanced and spiraled cyclonically inward. During 2100 UTC 1 January and 0600 UTC 2 January, as Isobel's center quickly moved southeastward, the inner end of the spiral rainband wrapped into the core region and organized into a new partial eyewall (Fig. 5). In addition, accompanied with the cyclonic inward propagation of the outer rainband was a cyclonic rotation of Isobel's track during 1500 UTC 1 January–0300 UTC 2 January (Fig. 3a). Isobel started to decay from 0600 UTC 2 January mainly as a result of the land effect as it was approaching the northwest coast of Australia (Fig. 3a).

6. Discussion on the influence of the MJO on Isobel's life cycle

Isobel's life cycle was closely related to the evolution of the MJO and the associated WWB in the simulation

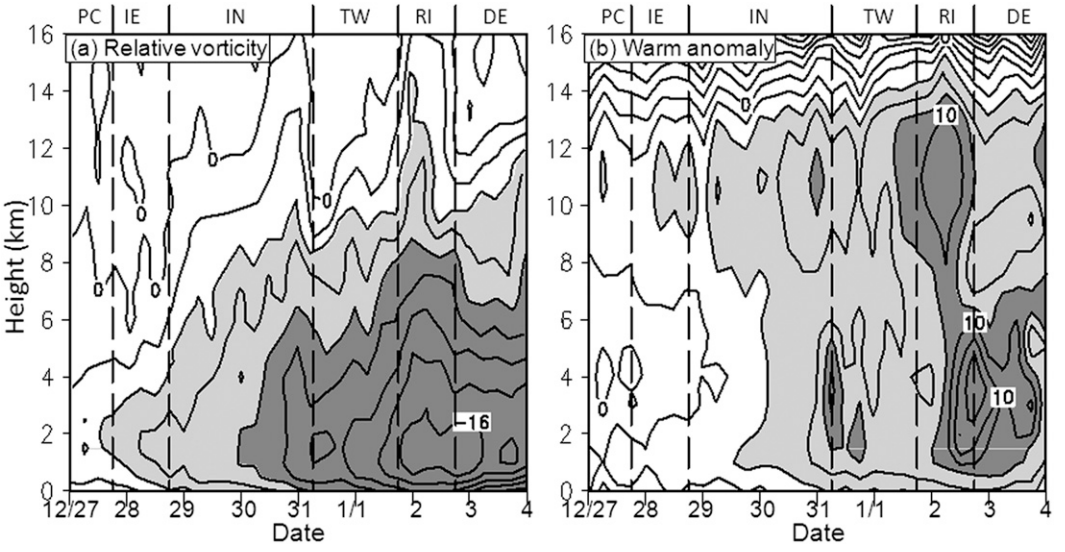

FIG. 11. Time–height cross section of (a) absolute vertical vorticity (10^{-5} s^{-1}) averaged within a radius of 301 km from Isobel's center and (b) potential temperature anomaly (K) averaged within a radius of 49 km. The contour interval in (a) is 2×10^{-5} s^{-1}, and light (dark) shading represents areas with vertical vorticity less than -4×10^{-5} s^{-1} (-8×10^{-5} s^{-1}). The contour interval in (b) is 2 K, and light (dark) shading represents areas with an anomaly greater than 4 K (8 K). The warm anomaly was defined as the difference from potential temperature averaged in 30°S–0° and 80°–140°E at 0000 UTC 23 Dec 2006.

as discussed in the last section. Hall et al. (2001) examined statistically the relationship between the TC activity and the MJO in the Australian region and found that the MJO strongly modulates the climatological pattern of TC geneses in the region, especially pronounced to the northwest of Australia, where Isobel formed. Previous studies also showed that the WWB associated with an MJO event could produce twin cyclones straddling the equator as a result of the Rossby wave response to the heating associated with the active convection phase of the MJO (Nitta et al. 1992; Sui and Lau 1992, Lin and Johnson 1996). The cyclonic gyre north of the equator, twin of Isobel, did not appear in this case. This might be due to the fact that convection associated with the MJO occurred around the Maritime Continent, mainly south of the equator. As a result, the WWB extended southeastward over the Timor Sea with convection suppressed in the Northern Hemisphere (Fig. 2) as predicted by the simple model of Gill (1980).

To examine how the large-scale circulation associated with the WWB as an external forcing contributed to the life cycle of Isobel, a composite analysis was executed. To eliminate the effects of the Maritime Continent, the signal of Isobel, and the southward movement of the WWB away from the equator, the composite analysis based on the basic wind fields was done for the period of 24–25 December 2006 when the WWB developed over the eastern Indian Ocean. Figure 14 shows the composite wind field with respect to the WWB center. The horizontal wind field is dominated by two large-scale zonally elongated cyclonic gyres: one to the north and one to the south of the WWB center (Figs. 14a,b). The large-scale cyclonic vorticity accompanied with the WWB with high CAPE provided favorable conditions for the initiation and development of small-scale/mesoscale convective vortices

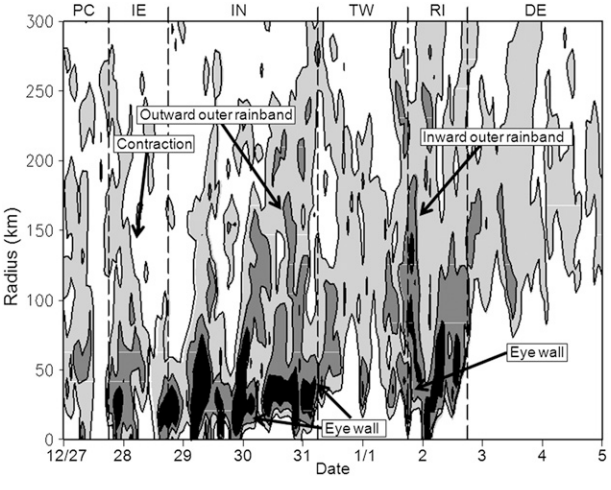

FIG. 12. Time–radius cross section of the azimuthal-mean rainfall rate (mm h^{-1}) based on 1.5-h model output. Areas with 10–20 mm h^{-1} are lightly shaded, those of 20–30 mm h^{-1} are heavily shaded, and those higher than 30 mm h^{-1} are filled.

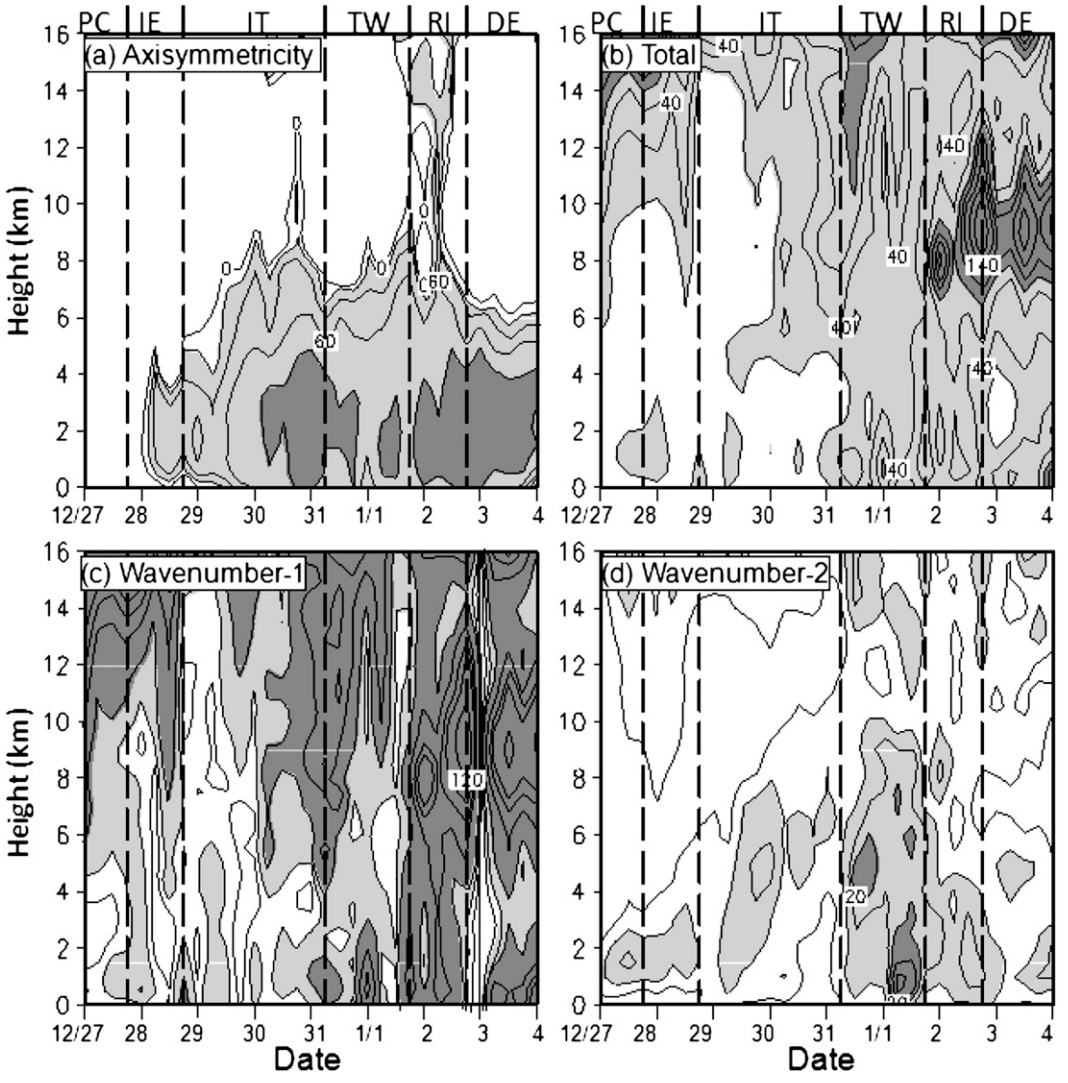

FIG. 13. (a) Time–height cross section of the axisymmetricity (%) defined in Eq. (2). Time–height cross section of (b) the total, (c) wavenumber-1, and (d) wavenumber-2 asymmetric kinetic energies ($m^2\ s^{-2}$) averaged within a radius of 301 km. The contour interval in (a) is 20% and light (dark) shading represents areas larger than 20% (80%). The contour interval in (b) is 20 $m^2\ s^{-2}$ and light (dark) shading represents areas larger than 20 $m^2\ s^{-2}$ (80 $m^2\ s^{-2}$). Contour intervals are 10 $m^2\ s^{-2}$ in (c) and 5 $m^2\ s^{-2}$ in (d) and light (dark) shading represents areas larger than 10 $m^2\ s^{-2}$ (20 $m^2\ s^{-2}$).

over the Java Sea and eventually led to the genesis of Isobel. Thus, the WWB associated with the MJO played an important role in the genesis and intensification of Isobel. Meanwhile, the WWB had a negative effect on the genesis of Isobel. During the early initial eddy stage, the vertical shear was strong over the initial eddies due to the low-level WWB and upper-level equatorial easterlies over the Java Sea (Figs. 7a, 8c, and 10), which is unfavorable for cyclogenesis (Gray 1968). The vertical shear decreased as the initial eddies moved southward away from the equator. Eddies then organized and developed into Tropical Storm Isobel over the Timor Sea.

The location of Isobel relative to the WWB center is important to the structure and intensity changes of the simulated Isobel. During the initial eddy stage and intensifying stage, Isobel was located southeast of the WWB center (Fig. 2f), where a strong large-scale convergence exists in the lower troposphere (Figs. 8b and 14c), favorable for the development of deep convection and the genesis of Isobel. In contrast, as the WWB moved southeastward, Isobel experienced a temporary weakening when Isobel was located southwest of the WWB center (Fig. 2f), where a strong stretching deformation and a strong large-scale divergence of zonal wind were dominant (Figs. 8a,b and

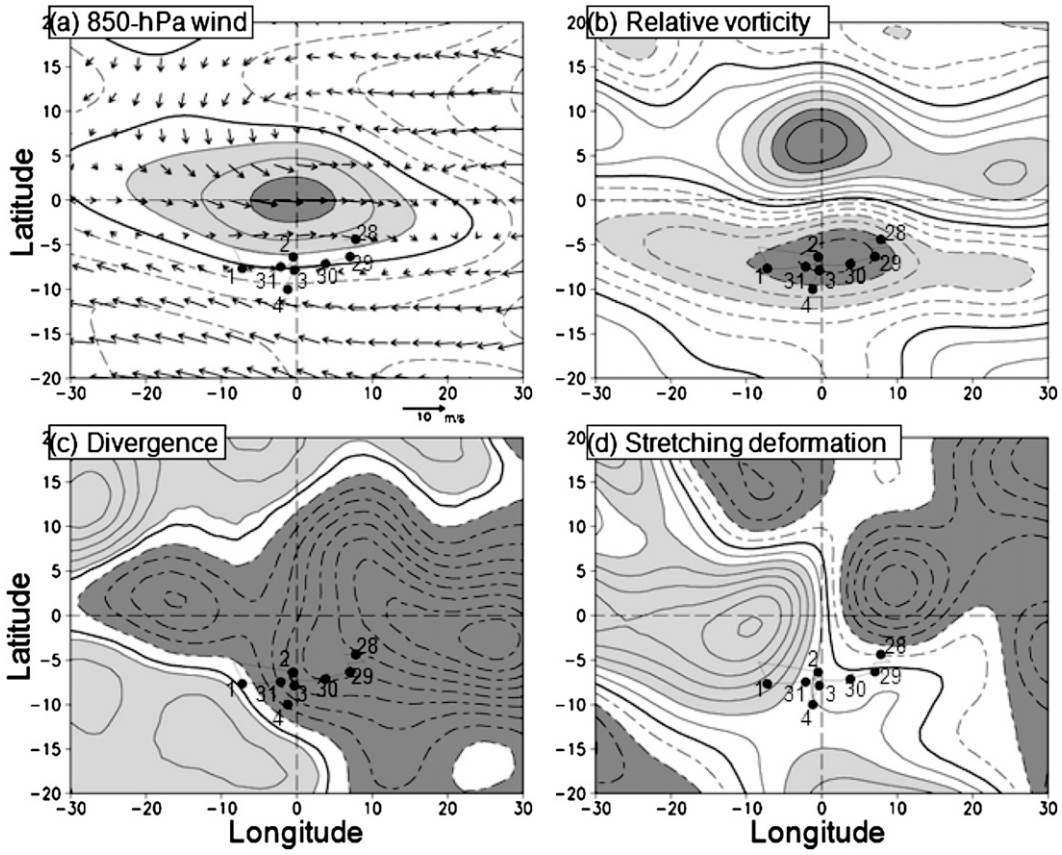

FIG. 14. Composite (a) horizontal winds (m s^{-1}), (b) relative vorticity (s^{-1}), (c) divergence (s^{-1}), and (d) stretching deformation (s^{-1}) based on the basic wind fields at 850 hPa with respect to the WWB center during 24–25 Dec 2006. The contour interval in (a) is 2 m s^{-1} and light (dark) shading represents areas larger than 2 m s^{-1} (6 m s^{-1}). The contour interval in (b) is 2×10^{-6} s^{-1} and light (dark) shading represents areas larger/lower than $\pm 6 \times 10^{-6}$ s^{-1} ($\pm 10 \times 10^{-6}$ s^{-1}). The contour interval in (c) is 2×10^{-7} s^{-1} and light (dark) shading represents areas larger (smaller) than 2×10^{-7} s^{-1} (-2×10^{-7} s^{-1}). The contour interval in (d) is 1×10^{-6} s^{-1} and light (dark) shading represents areas larger (smaller) than 2×10^{-6} s^{-1} (-2×10^{-6} s^{-1}). Solid (dashed) contours denote positive (negative) values. Track of Isobel relative to the WWB center and locations at 0000 UTC are shown by solid line and closed circles (as in Fig. 2f).

14d). The strong stretching deformation was responsible for the development of two spiral rainbands (Fig. 5) and a wavenumber-2 asymmetric dynamical structure (Fig. 13d) in the late temporary weakening stage. This differs from the dominant wavenumber-1 asymmetry developed in the strong vertical shear in the early weakening stage.

Davis et al. (2008) analyzed the tropical cyclogenesis over the eastern Pacific in 2005 and 2006 and found that the horizontal stretching deformation in the background flow at 900 hPa differed significantly between the developing and nondeveloping systems. Developing systems were generally located in the zero or negative stretching deformation field while nondeveloping systems mostly occurred in the positive stretching deformation field. The structures of nondeveloping systems were generally zonally elongated in the strong stretching deformation field, which was very similar to the wavenumber-2 asymmetric structure developed in Isobel in the late temporary weakening stage in our simulation. Although Davis et al. (2008) did not analyze TCs at the mature stage, the strong horizontal stretching deformation in the environmental flow may have a negative effect on TC intensity by triggering convective asymmetries in the inner core. Therefore, depending on the location of Isobel relative to the WWB center, the MJO played both positive and negative effects on the genesis and intensity of the simulated Isobel.

7. Conclusions

The global cloud-system-resolving model NICAM successfully simulated the major features of Isobel's life cycle in an MJO experiment. This allowed us to investigate the effect of the MJO on the evolution of the simulated Isobel, as summarized in Table 1. With high CAPE around the Maritime Continent, the WWB over the Java Sea associated with the MJO onset over the East Indian

Ocean enhanced the large-scale cyclonic vorticity and convergence in the lower troposphere, favorable for active convection, leading to the development of a zonally elongated rainband (the preconditioning stage of Isobel). Convective eddies initiated and organized in the rainband in the preconditioned environment (the initial eddy stage). As the WWB extended eastward, the initial eddies moved southeastward. After the initial eddies arrived at the favorable environment with weak vertical shear and horizontal cyclonic shear enhanced between the WWB and easterly trade winds over the Timor Sea, Isobel developed the typical TC structure (the intensifying stage). With the increase in vertical shear, a wavenumber-1 asymmetric structure developed in Isobel's eyewall, leading to a breakdown of the eyewall and a temporary weakening of the storm (the early temporary weakening stage). As Isobel shifted to the west of the WWB center, the wavenumber-2 asymmetric structure in the inner core of Isobel was excited in a strong environmental stretching deformation field in the mid–lower troposphere (the late temporary weakening stage). As Isobel quickly moved southeastward, it experienced an eyewall reformation process through the axisymmetrization of an inward-propagating outer rainband that formed downwind of the WWB center (the reintensifying stage). Isobel finally weakened as a result of the land effect as it approached the northwest coast of Australia (the decaying stage).

The life cycle of the simulated Isobel therefore was largely controlled by a large-scale environmental condition characterized by the MJO onset and the associated WWB, the easterly trade winds, and changes in vertical shear and the steering flow. The WWB associated with the MJO, on one hand, contributed positively to the intensification of Isobel as Isobel was located southeast of the WWB center where large-scale convergence occurred, and on the other hand, affected negatively on Isobel's development as Isobel was located southwest of the WWB center where the environmental stretching deformation was strong. Therefore, the MJO had both positive and negative effects on the intensity of the simulated Isobel, depending on the relative location of Isobel and the WWB center associated with the MJO.

Although the NICAM MJO experiment provides high temporal and spatial resolution dataset for a detailed study of the multiscale interactions involved in the life cycle of the simulated Isobel, the results reported here should not be taken to imply that there is skill at forecasting TC behavior at such a lead time. We noticed that the simulated Isobel was stronger than the observed owing to the stronger MJO in the simulation. Nevertheless, to understand the multiscale interactions involved in the simulated Isobel can help understand the role of the MJO in the life cycle of a TC. Therefore, the difference in the simulated storm intensity from that observed should not be a big problem for our purpose in this study. This paper covers only the evolution of the large-scale environmental flow and the storm-scale evolution of Isobel. The multiscale interactions among the large-scale, storm-scale, and mesoscale processes in the simulated Isobel will be discussed in Part II.

Acknowledgments. The authors are grateful to Dr. Ping Liu for his helpful comments on the NICAM-simulated MJO verification. This study was supported in part by NSF Grant ATM-0754039 and in part by JAMSTEC, NASA, and NOAA through their sponsorships of the International Pacific Research Center (IPRC) in the School of Ocean and Earth Science and Technology (SOEST) at the University of Hawaii. Part of this study was also supported by the JST/CREST in Japan. The Earth Simulator was used for the NICAM simulation.

REFERENCES

Barrett, B. S., and M. L. Lance, 2009: Links between tropical cyclone activity and Madden–Julian oscillation phase in the North Atlantic and Northeast Pacific basins. *Mon. Wea. Rev.,* **137,** 727–744.

Bender, M. A., 1997: The effect of relative flow on the asymmetric structure in the interior of hurricanes. *J. Atmos. Sci.,* **54,** 703–724.

Bessafi, M., and M. C. Wheeler, 2006: Modulation of south Indian Ocean tropical cyclones by the Madden–Julian oscillation and convectively coupled equatorial waves. *Mon. Wea. Rev.,* **134,** 638–656.

Black, M. L., J. F. Gamache, F. D. Marks, C. E. Samsury, and H. E. Willoughby, 2002: Eastern Pacific Hurricanes Jimena of 1991 and Olivia of 1994: The effect of vertical shear on structure and intensity. *Mon. Wea. Rev.,* **130,** 2291–2312.

Briegel, L. M., and W. M. Frank, 1997: Large-scale influences on tropical cyclogenesis in the western North Pacific. *Mon. Wea. Rev.,* **125,** 1397–1413.

Chelton, D. B., and M. H. Freilich, 2005: Scatterometer-based assessment of 10-m wind analyses from the operational ECMWF and NCEP numerical weather prediction models. *Mon. Wea. Rev.,* **133,** 409–429.

Davis, C., C. Snyder, and A. C. Didlake, 2008: A vortex-based perspective of eastern Pacific tropical cyclone formation. *Mon. Wea. Rev.,* **136,** 2461–2477.

Dickinson, M., and J. Molinari, 2002: Mixed Rossby–gravity waves and western Pacific tropical cyclogenesis. Part I: Synoptic evolution. *J. Atmos. Sci.,* **59,** 2183–2196.

Frank, W. M., and E. A. Ritchie, 1999: Effects of environmental flow upon tropical cyclone structure. *Mon. Wea. Rev.,* **127,** 2044–2061.

——, and ——, 2001: Effects of vertical wind shear on the intensity and structure of numerically simulated hurricanes. *Mon. Wea. Rev.,* **129,** 2249–2269.

——, and P. E. Roundy, 2006: The role of tropical waves in tropical cyclogenesis. *Mon. Wea. Rev.,* **134,** 2397–2417.

Freilich, M. H., and R. S. Dunbar, 1999: The accuracy of the NSCAT 1 vector winds: Comparisons with National Data Buoy Center buoys. *J. Geophys. Res.,* **104,** 11 231–11 246.

Fudeyasu, H., Y. Wang, M. Satoh, T. Nasuno, H. Miura, and W. Yanase, 2008: Global cloud-system-resolving model NICAM successfully simulated the lifecycles of two real tropical cyclones. *Geophys. Res. Lett.,* **35,** L22808, doi:10.1029/2008GL036003.

——, ——, ——, ——, ——, and ——, 2010: Multiscale interactions in the life cycle of a tropical cyclone simulated in a global cloud-system-resolving model. Part II: System-scale and mesoscale processes. *Mon. Wea. Rev.,* **138,** 4305–4327.

Gill, A. E., 1980: Some simple solutions for heat-induced tropical circulation. *Quart. J. Roy. Meteor. Soc.,* **106,** 447–462.

Grabowski, W. W., 1998: Toward cloud resolving modeling of large-scale tropical circulations: A simple cloud microphysics parameterization. *J. Atmos. Sci.,* **55,** 3283–3298.

Gray, W. M., 1968: Global view of the origin of tropical disturbances and storms. *Mon. Wea. Rev.,* **96,** 669–700.

——, 1979: Hurricanes: Their formation, structure and likely role in the general circulation. *Meteorology over the Tropical Oceans,* D. B. Shaw, Ed., Royal Meteorological Society, 155–218.

Hall, J. D., A. J. Matthews, and D. J. Karoly, 2001: The modulation of tropical cyclone activity in the Australian region by the Madden–Julian oscillation. *Mon. Wea. Rev.,* **129,** 2970–2982.

Harrison, D. E., and G. A. Vecchi, 1997: Westerly wind events in the tropical Pacific, 1986–95. *J. Climate,* **10,** 3131–3156.

Heymsfield, G. M., J. Halverson, E. Ritchie, J. Simpson, J. Molinari, and L. Tian, 2006: Structure of highly sheared Tropical Storm Chantal during CAMEX-4. *J. Atmos. Sci.,* **63,** 268–287.

Kurihara, Y., M. A. Bender, R. E. Tuleya, and R. J. Ross, 1990: Prediction experiments of Hurricane Gloria (1985) using a multiply nested movable mesh model. *Mon. Wea. Rev.,* **118,** 2185–2198.

Landsea, C. W., 1993: A climatology of intense (or major) Atlantic hurricanes. *Mon. Wea. Rev.,* **121,** 1703–1713.

Liebmann, B., H. H. Hendon, and J. D. Glick, 1994: The relationship between tropical cyclones of the western Pacific and Indian Oceans and the Madden–Julian oscillation. *J. Meteor. Soc. Japan,* **72,** 401–412.

Lin, X., and R. H. Johnson, 1996: Heating, moistening, and rainfall over the western Pacific warm pool during TOGA COARE. *J. Atmos. Sci.,* **53,** 3367–3383.

Liu, P., and Coauthors, 2009: An MJO simulated by the NICAM at 14- and 7-km resolution. *Mon. Wea. Rev.,* **137,** 3254–3268.

Liu, Y. B., D. L. Zhang, and M. K. Yau, 1997: Multiscale numerical study of Hurricane Andrew (1992). Part I: Explicit simulation and verification. *Mon. Wea. Rev.,* **125,** 3073–3093.

Madden, R. A., and P. R. Julian, 1971: Detection of a 40–50-day oscillation in the zonal wind in the tropical Pacific. *J. Atmos. Sci.,* **28,** 702–708.

——, and ——, 1972: Detection of global-scale circulation cells in the tropics with a 40–50-day period. *J. Atmos. Sci.,* **29,** 1109–1123.

——, and ——, 1994: Observations of the 40–50-day tropical oscillation—A review. *Mon. Wea. Rev.,* **122,** 814–837.

Maloney, E. D., and D. L. Hartmann, 2000a: Modulation of eastern North Pacific hurricanes by the Madden–Julian oscillation. *J. Climate,* **13,** 1451–1460.

——, and ——, 2000b: Modulation of hurricane activity in the Gulf of Mexico by the Madden–Julian oscillation. *Science,* **287,** 2002–2004.

——, and ——, 2001: The Madden–Julian oscillation, barotropic dynamics, and North Pacific tropical cyclone formation. Part I: Observations. *J. Atmos. Sci.,* **58,** 2545–2558.

Masunaga, H., M. Satoh, and H. Miura, 2008: A joint satellite and global cloud-resolving model analysis of a Madden–Julian Oscillation event: Model diagnosis. *J. Geophys. Res.,* **113,** D17210, doi:10.1029/2008JD009986.

McBride, J. L., and R. Zehr, 1981: Observational analysis of tropical cyclone formation. Part II: Comparison of nondeveloping versus developing systems. *J. Atmos. Sci.,* **38,** 1132–1151.

Merrill, R. T., 1988: Environmental influences on hurricane intensification. *J. Atmos. Sci.,* **45,** 1678–1687.

Miura, H., M. Satoh, T. Nasuno, A. T. Noda, and K. Oouchi, 2007: A Madden–Julian Oscillation event realistically simulated by a global cloud-resolving model. *Science,* **318,** 1763–1765.

——, ——, ——, ——, and ——, 2008: Response of coarse-resolution models only partly cloudy. *Science,* **320,** 613.

Molinari, J., and D. Vollaro, 2000: Planetary- and synoptic-scale influences on eastern Pacific tropical cyclogenesis. *Mon. Wea. Rev.,* **128,** 3296–3307.

Murakami, T., and W. L. Sumathipala, 1989: Westerly bursts during the 1982/83 ENSO. *J. Climate,* **2,** 71–85.

Nakanishi, M., and H. Niino, 2006: An improved Mellor–Yamada level-3 model: Its numerical stability and application to a regional prediction of advection fog. *Bound.-Layer Meteor.,* **119,** 397–407.

Nasuno, T., H. Tomita, S. Iga, H. Miura, and M. Satoh, 2007: Multiscale organization of convection simulated with explicit cloud processes on an aquaplanet. *J. Atmos. Sci.,* **64,** 1902–1921.

——, H. Miura, M. Satoh, A. T. Noda, and K. Oouchi, 2009: Multi-scale organization of convection in a global numerical simulation of the December 2006 MJO event using explicit moist processes. *J. Meteor. Soc. Japan,* **87,** 335–345.

Nitta, T., T. Mizuno, and K. Takahashi, 1992: Multiscale convective systems during the initial phase of the 1986/87 El Niño. *J. Meteor. Soc. Japan,* **70,** 447–466.

Reynolds, R. W., and T. M. Smith, 1994: Improved global sea surface temperature analyses using optimum interpolation. *J. Climate,* **7,** 929–948.

Ritchie, E. A., and G. J. Holland, 1999: Large-scale patterns associated with tropical cyclogenesis in the western Pacific. *Mon. Wea. Rev.,* **127,** 2027–2043.

Satoh, M., T. Matsuno, H. Tomita, H. Miura, T. Nasuno, and S. Iga, 2008: Nonhydrostatic icosahedral atmospheric model (NICAM) for global cloud resolving simulations. *J. Comput. Phys.,* **227,** 3486–3514.

Seiki, A., and Y. N. Takayabu, 2007: Westerly wind bursts and their relationship with intraseasonal variations and ENSO. Part I: Statistics. *Mon. Wea. Rev.,* **135,** 3325–3345.

Simpson, R. H., and H. Riehl, 1958: Mid-tropospheric ventilation as a constraint on hurricane development and maintenance. *Proc. 10th Conf. on Hurricanes,* Miami Beach, FL, Amer. Meteor. Soc., D4.1–D4.10.

Sui, C. H., and K. M. Lau, 1992: Multiscale phenomena in the tropical atmosphere over the western Pacific. *Mon. Wea. Rev.,* **120,** 407–430.

Thorncroft, C., and K. Hodges, 2001: African easterly wave variability and its relationship to Atlantic tropical cyclone activity. *J. Climate,* **14,** 1166–1179.

Tomita, H., and M. Satoh, 2004: A new dynamical framework of nonhydrostatic global model using the icosahedral grid. *Fluid Dyn. Res.,* **34,** 357–400.

Wang, Y., 2002a: Vortex Rossby waves in a numerically simulated tropical cyclone. Part I: Overall structure, potential vorticity, and kinetic energy budgets. *J. Atmos. Sci.,* **59,** 1213–1238.

——, 2002b: Vortex Rossby waves in a numerically simulated tropical cyclone. Part II: The role in tropical cyclone structure and intensity changes. *J. Atmos. Sci.,* **59,** 1239–1262.

——, 2007: A multiply nested, movable mesh, fully compressible, nonhydrostatic tropical cyclone model-TCM4: Model description and development of asymmetries without explicit asymmetric forcing. *Meteor. Atmos. Phys.,* **97,** 93–116.

——, 2008: Structure and formation of an annular hurricane simulated in a fully compressible, nonhydrostatic model—TCM4. *J. Atmos. Sci.,* **65,** 1505–1527.

——, and G. J. Holland, 1996: Tropical cyclone motion and evolution in vertical shear. *J. Atmos. Sci.,* **53,** 3313–3332.

——, and C. C. Wu, 2004: Current understanding of tropical cyclone structure and intensity changes—A review. *Meteor. Atmos. Phys.,* **87,** 257–278.

——, M. T. Montgomery, and B. Wang, 2004: How much vertical shear can a tropical cyclone resist? *Bull. Amer. Meteor. Soc.,* **85,** 661–662.

Willoughby, H. E., J. A. Clos, and M. G. Shoreibah, 1982: Concentric eye walls, secondary wind maxima, and the evolution of the hurricane vortex. *J. Atmos. Sci.,* **39,** 395–411.

Zehr, R., 1992: Tropical cyclogenesis in the western North Pacific. NOAA Tech. Rep. NESDIS 61, 181 pp.

Zeng, Z.-H., Y. Wang, and C.-C. Wu, 2007: Environmental dynamical control of tropical cyclone intensity—An observational study. *Mon. Wea. Rev.,* **135,** 38–59.

——, L.-S. Chen, and Y. Wang, 2008: An observational study of environmental dynamical control of tropical cyclone intensity in the Atlantic. *Mon. Wea. Rev.,* **136,** 3307–3322.

Zhang, C., 2005: Madden-Julian Oscillation. *Rev. Geophys.,* **43,** RG2003, doi:10.1029/2004RG000158.